

Dense Inhibitory Connectivity in Neocortex

Elodie Fino^{1,*} and Rafael Yuste¹

¹Howard Hughes Medical Institute, Department of Biological Sciences, Columbia University, New York, NY 10027, USA

*Correspondence: ef2308@columbia.edu

DOI 10.1016/j.neuron.2011.02.025

SUMMARY

The connectivity diagram of neocortical circuits is still unknown, and there are conflicting data as to whether cortical neurons are wired specifically or not. To investigate the basic structure of cortical microcircuits, we use a two-photon photostimulation technique that enables the systematic mapping of synaptic connections with single-cell resolution. We map the inhibitory connectivity between upper layers somatostatin-positive GABAergic interneurons and pyramidal cells in mouse frontal cortex. Most, and sometimes all, inhibitory neurons are locally connected to every sampled pyramidal cell. This dense inhibitory connectivity is found at both young and mature developmental ages. Inhibitory innervation of neighboring pyramidal cells is similar, regardless of whether they are connected among themselves or not. We conclude that local inhibitory connectivity is promiscuous, does not form subnetworks, and can approach the theoretical limit of a completely connected synaptic matrix.

INTRODUCTION

The neocortex is the largest part of the mammalian brain, yet its function is still poorly understood. Anatomical and physiological studies have emphasized the vertical (or “columnar”) nature of its connectivity (Hubel and Wiesel, 1977; Lorente de Nó, 1949; Mountcastle, 1982), giving rise to the proposal that the neocortex is composed of repetitions of a basic modular unit, performing essentially the same computation on different inputs (Douglas et al., 2004; Hubel and Wiesel, 1974; Lorente de Nó, 1949; Mountcastle, 1982). Consistent with this hypothesis, in different species and cortical areas, the cortex develops in a stereotypical fashion (Katz and Shatz, 1996) with similar interlaminar connections (Burkhalter, 1989; Douglas et al., 2004; Gilbert and Wiesel, 1979). At the same time, there are structural differences among cortical areas and species (DeFelipe, 1993), so each cortical region could still have a specific, dedicated circuit. Crucial to this debate is the knowledge of how different subtypes of cortical neurons connect to each other, an issue for which there is only scant available data. Although some studies find great specificity in cortical connections (Callaway, 1998; Hubel, 1988; Thomson and Lamy, 2007), others have proposed that cortical neurons connect without any specificity

(Braitenberg and Schüz, 1991; Peters and Jones, 1984), forming perhaps a neural network, or a “tabula rasa,” on which activity-dependent developmental rules could sculpt mature circuits (Kalisman et al., 2005; Rolls and Treves, 1998; Stepanyants et al., 2002).

To measure the specificity in cortical connections, one would need techniques that reveal synaptically connected neurons. In the last decade, electrophysiological recordings from connected cortical neurons in brain slices (Thomson et al., 1988) have demonstrated many intra- and interlaminar connections between specific neuronal subtypes (Deuchards et al., 1994; Feldmeyer and Sakmann, 2000; Markram et al., 1997). If the goal, however, is to eventually reveal most, or all, connections within a given area, this method is limited given the few connections that can be tested in one experiment. To circumvent this problem, we designed an optical technique, a modification of one-photon photostimulation (Callaway and Katz, 1993), that reveals synaptic connections in large numbers and can provide a map of most connections to a neuron in a local area, with single-cell resolution (Nikolenko et al., 2007). Using two-photon uncaging of glutamate in brain slices, one can sequentially activate hundreds of potential presynaptic cells, one by one, and quickly test whether they are connected to a given postsynaptic neuron (Nikolenko et al., 2007).

We were interested to apply this two-photon mapping technique to inhibitory circuits and determine the functional structure of inhibitory networks in the neocortex. The cortex has numerous types of GABAergic interneurons (Fairen et al., 1984), which play a determinant role in the regulation of the excitability of pyramidal cells (PCs) and the activity of cortical microcircuits, by controlling different parts of the axo-dendritic arborization of the PCs (Somogyi et al., 1998). One can distinguish many subtypes of inhibitory neurons in neocortical circuits morphologically and physiologically (Gupta et al., 2000; Ascoli et al., 2008; Yuste, 2005). For this study, we focused on dendritic targeting inhibitory cells, the somatostatin-expressing interneurons (Kawaguchi and Kubota, 1997; Wang et al., 2004), which represent approximately 30% of the neocortical interneurons in mouse (Gonchar and Burkhalter, 1997). Somatostatin-positive cells are composed of several subtypes, of which Martinotti neurons are the predominant type (Halabisky et al., 2006; McGarry et al., 2010). They generally, although not always (Gonchar et al., 2002), contact apical and tufted dendrites of PCs (Kawaguchi and Kubota, 1997; Wang et al., 2004). Somatostatin-positive interneurons display low-threshold spiking (Kawaguchi, 1995), generating a global dendritic calcium spike (Goldberg et al., 2004), and can fire spontaneously in a pacemaker fashion, in the absence of any synaptic input (LeBon-Jego and Yuste, 2007). Within neuronal circuits, they control local synaptic inputs of PCs

(Murayama et al., 2009; Silberberg and Markram, 2007) and are recruited by network activity (Kapfer et al., 2007), to the point that they can be activated by a single PC (Kozloski et al., 2001), mediating a strong disinhibitory inhibition between PCs (Silberberg and Markram, 2007).

These specific morphological and physiological properties suggest that somatostatin-positive interneurons implement a specific function in the microcircuit. However, understanding how exactly they are integrated into the network has remained elusive and is a key step to determine their exact role. Their connectivity patterns have mainly been explored with paired recordings, characterizing uni- or bidirectional synaptic contacts with PCs or with one-photon photostimulation experiments (Katzel et al., 2010; Otsuka and Kawaguchi, 2009; Thomson and Lamy, 2007; Xu and Callaway, 2009; Yoshimura and Callaway, 2005). In spite of these studies, it is still not clear how exactly do somatostatin-positive interneurons connect to the local population of targets, and whether their connections are specific or not.

Here, we characterize the synaptic connectivity between a local population of somatostatin-positive interneurons and their PC targets within layer 2/3 in frontal cortex. Using laser multiplexing, and a new caged glutamate compound, on brain slices from a mouse strain where somatostatin neurons are labeled with GFP, we build maps of connected interneuron-PCs, with single-cell resolution. We find a high degree of local connectivity, at both early and mature stages of circuit development, without any evidence for specific synaptic subcircuits. Surprisingly, some maps demonstrate a completely connected local network, something that, to our knowledge, has not been reported before in CNS circuits. An all-to-all connectivity has implications for models of cortical modularity and processing.

RESULTS

Two-Photon Photostimulation of Somatostatin-Positive Interneurons

Our goal was to study the connectivity from a defined type of neocortical interneurons to PCs. To identify a homogeneous population of interneurons in living slices, we used a transgenic mouse strain that express GFP exclusively in somatostatin interneurons (Oliva et al., 2000) and chose the upper layers from frontal cortex, because of its abundance of GFP cells (Figure 1A). In these mice, all recorded GFP cells from were interneurons, as defined by nonpyramidal structural or functional characteristics ($n = 55$). Morphologically, GFP cells had ascending axonal arborizations with extensive branching in layer 1 and horizontal collaterals, typical of Martinotti cells (Figure 1B; Halabisky et al., 2006; McGarry et al., 2010; Wang et al., 2004). Electrophysiologically, GFP cells had a marked afterhyperpolarization, a moderate frequency of discharge (32.1 ± 2.2 Hz, $n = 35$), a significant spike frequency adaptation (0.49 ± 0.02 , $n = 35$) and a relatively linear I/V curve (Figure 1C and Table 1). These results confirmed that GFP cells were somatostatin-positive interneurons (Halabisky et al., 2006; McGarry et al., 2010; Oliva et al., 2000; Wang et al., 2004). In fact, using cluster analysis, most recorded GFP cells (30 out of 38 cells) belonged to the Martinotti subtype, as defined by their morphological or electrophysiological characteristics (McGarry et al., 2010).

We set out to map inputs from layer 2/3 somatostatin-positive interneurons ("sGFP" cells, for the rest of the study), onto local pyramidal neurons (PCs), identified by their somatic morphologies. For this, we adapted the two-photon photostimulation technique to build single-cell resolution connectivity maps. While the original two-photon mapping method used MNI-glutamate as the caged compound (Matsuzaki et al., 2004; Nikolenko et al., 2007), we found that, at concentrations needed for effective two-photon uncaging, MNI-glutamate completely blocks GABAergic transmission (Fino et al., 2009). To circumvent this problem, we developed a new caged glutamate, RuBi-Glutamate, which has higher quantum yield and can therefore be used at lower concentrations, enabling the optical mapping of inhibitory connections (Fino et al., 2009). With a similar laser multiplexing uncaging protocol previously used to activate PCs (Fino et al., 2009), we were able to uncage RuBi-Glutamate and fire individual sGFP cells (Figure 1D). Two-photon RuBi-Glutamate photoactivation was reliable: repetitive photostimulation of the same neuron with the same laser power evoked the same number of action potentials (APs) (Figure 1E).

Before mapping, we first performed simultaneous whole-cell recordings from pairs of connected sGFP interneurons and PCs to characterize their typical inhibitory monosynaptic connections and used that information to design the optimal protocols to be able to identify them in photostimulation experiments. To better detect potential monosynaptic IPSCs, we performed all recordings from PCs in voltage clamp. Because somatostatin-positive interneurons normally target more distal dendrites of PCs (Kawaguchi and Kubota, 1997), we used a Cs-based internal solution and also enhanced the amplitude of IPSCs by clamping the postsynaptic PC at +40 mV. Inhibitory synaptic inputs were thus recorded as outward currents (Figure 1F). Monosynaptic IPSCs had average latencies of 1.34 ± 0.11 ms and amplitudes of 39.30 ± 9.48 pA ($n = 15$; Table 2). In addition, evoking 2 APs at 40 Hz in the sGFP cell revealed mainly depressing synapses ($75.57 \pm 7.45\%$, $n = 15$). With these paired recordings, we confirmed that the IPSCs measured in postsynaptic PCs after evoking an AP in sGFP neurons were similar to those observed after photoactivation of the same neuron by RuBi-Glutamate uncaging (Figure 1G). We also used paired recordings to characterize potential side effects of RuBi-Glutamate and did not observe any significant effect on passive and active membrane properties of the sGFP cells (Table 1) or on the synaptic transmission between sGFP cells and PCs (Table 2). But because of our previous observations (Fino et al., 2009), we also characterized the effect of RuBi-Glutamate on GABAergic currents by patching pairs in control condition and then adding RuBi-Glutamate to the bath (Figure 1H₁; Fino et al., 2009). At the concentration used in this study (300 μ M), RuBi-Glutamate blocked $47.7\% \pm 10.8\%$ ($n = 7$) of the monosynaptic IPSCs (Figure 1H₂). Nevertheless, we were still able to detect weak inhibitory connections by evoking a burst of APs in the sGFP interneuron rather than a single AP (Figure 1I; $n = 3$).

Two-Photon Mapping of Inhibitory Connections

We then used two-photon RuBi-Glutamate uncaging to systematically map the connections from sGFP interneurons onto PCs. We first imaged fields of sGFP interneurons and patched a layer

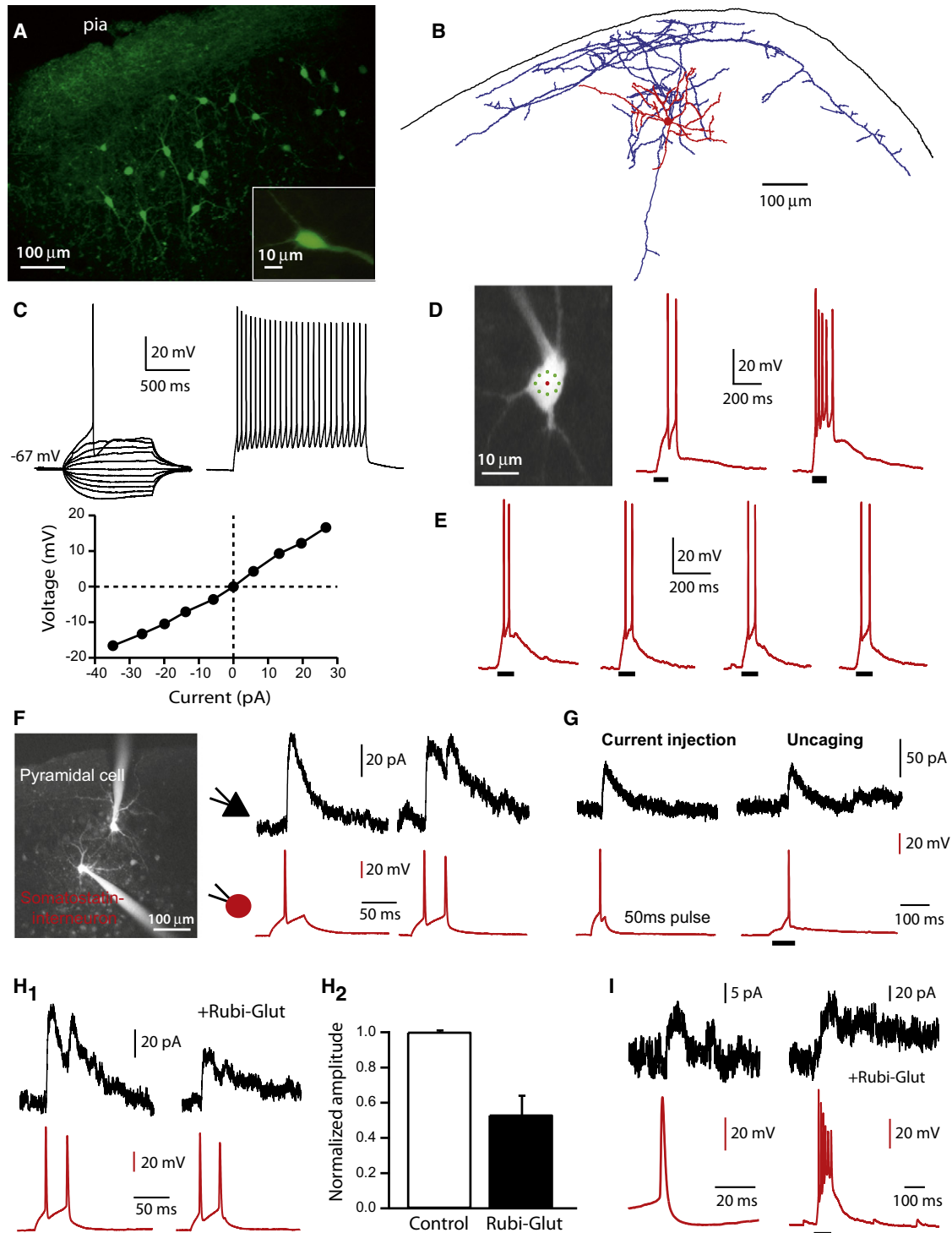


Figure 1. Two-Photon Activation of Somatostatin-Expressing Interneurons

(A) Somatostatin-expressing interneurons in a Z stack of a slice from GFP-expressing mice.

(B) Reconstruction of a sGFP interneuron, which is a Martinotti cell. Dendrites are in red and axons in blue. Note the wide axonal arborization, projecting to the pia (black line).

(C) Electrophysiological characteristics of somatostatin interneuron. Traces show individual voltage responses to series of 1 s from -35 pA to $+35$ pA (left panel; note the sag for hyperpolarizing steps) and to twice the rheobase (right panel, spike frequency = 21 Hz). I/V curve (lower panel), measured at the steady-state of the voltage steps.

Table 1. Electrophysiological Properties of sGFP Interneurons and Lack of Effect of RuBi-Glutamate

	Control (n = 24)	Rubi-Glutamate (n = 11)	Statistics
RMP (mV)	-65.04 ± 0.63	-66.27 ± 0.81	ns
Ri (MΩ)	449.38 ± 30.67	380.00 ± 26.57	ns
Rheobase (pA)	38.54 ± 6.28	48.63 ± 8.83	ns
AP threshold	-39.21 ± 1.82	-41.08 ± 2.01	ns
AP amplitude (mV)	64.68 ± 2.92	60.98 ± 2.21	ns
AP duration (ms)	3.57 ± 0.22	4.89 ± 0.43	p < 0.05
Initial frequency (Hz)	32.06 ± 2.74	32.27 ± 4.31	ns
Final frequency (Hz)	15.15 ± 1.08	13.82 ± 1.45	ns
SFA	0.51 ± 0.03	0.47 ± 0.06	ns

RMP, resting membrane potential; Ri, input resistance; AP, action potential; SFA, spike frequency adaptation.

2/3 PC, usually at the border of layers 1 and 2/3, and placed uncaging laser targets onto the somata of each of the sGFP interneurons in the field of view (Figure 2A). We then sequentially stimulated them with two-photon RuBi-Glutamate uncaging, while recording responses evoked in the PC. sGFP cells were stimulated several times, with different laser powers, with the PC held at either +40 or -40 mV (Figure 2A). This protocol was chosen for two reasons. First, clamping the PC at +40 mV increased the chloride driving force, which allowed us to better detect inhibitory connections, including weaker ones. Second, switching between +40 mV and -40 mV allowed us to distinguish inhibitory, chloride-based responses, which did not reverse sign, from contaminating glutamatergic responses, whose reversal potential is around 0 mV and which therefore switched polarity. This switching test was necessary because, occasionally, two-photon glutamate uncaging of an inhibitory cell resulted in a paradoxical glutamatergic response, which we termed “false-positive” responses. These false positives might arise from direct activation of processes of the recorded PCs (see Nikolenko et al., 2007). Indeed, one can distinguish them from true positives (i.e., real synaptic inhibitory connections) based on the kinetics and latency of the responses (Figure 2B and see Figure S1 available online). In fact, to evoke an AP with two-photon glutamate uncaging, one usually needs a substantial accumulation of glutamate to lead to a sufficient activation of the glutamatergic receptors and firing of the cell (Figure S1A). This results in a longer latency between the onset

Table 2. Characteristics of Synaptic Transmission between sGFP Interneurons and Layer 2/3 Pyramidal Cells; Lack of Effect of RuBi-Glutamate

	Control (n = 15)	Rubi-Glut (n = 13)	Statistics
Latency (ms)	1.34 ± 0.11	1.48 ± 0.26	ns
Rise time (ms)	8.33 ± 0.70	6.94 ± 0.83	ns
Amplitude (pA)	39.30 ± 9.48	25.65 ± 9.27	ns
Rate of rise (pA/ms)	5.67 ± 1.39	4.12 ± 1.89	ns
Pot/Dep (%)	75.57 ± 7.45	80.75 ± 9.44	ns
Summation (%)	125.66 ± 7.24	127.06 ± 8.15	ns
Failure rate (%)	4.42 ± 2.09	8.41 ± 5.90	ns

Pot/Dep, potentiation/depression.

of the laser pulse and the evoked AP. In agreement with this, the latency of connected interneurons was significantly longer than latency of false positives, glutamatergic responses (Figures S1B–S1D; 48.54 ± 0.91 , $n = 576$ for connected interneurons versus 22.21 ± 1.22 , $n = 164$ for false positives; $p < 0.001$, Mann-Whitney test). This is consistent with the hypothesis that the faster false-positive responses arise from direct stimulation of the dendritic arborization of the recorded PCs. Confirming this, the differences in delay kinetics between false and true positives matched the “switching test” results to identify true connected interneurons, as those responses which had slower kinetics at +40 mV were the ones that switched from outward to inward currents at -40 mV.

We also wondered whether we could mistakenly assign true positive statuses to neighboring unconnected sGFP cells, if they were inadvertently stimulated by the uncaging protocol. In order to test whether we activated other interneuron in the field, aside from the targeted one, we performed additional control experiments in which we recorded sGFP cells in current-clamp and uncaged over every other sGFP cells around it. In 81% of the cases ($n = 16$), we did not detect any unspecific activation of the recorded sGFP cell. The remaining 19% of interneurons displayed mainly a subthreshold activation with the laser power used for mapping experiments (Figures S2A and S2B). Even interneurons located next to the stimulated one were not activated by the uncaging (Figures S2C and S2D). This indicates that the uncaging needs to be performed over the soma to be able to fire the interneurons. These control experiments therefore demonstrated that the responses from the stimulation of an individual sGFP cell were not

(D) sGFP interneuron and position of the multiplexed two-photon uncaging targets (8 subtargets; green) on the soma of the cell. In this example, two (left) or a burst (right) of APs were evoked with 180 mW and 250 mW on sample, respectively. Black lines indicate uncaging pulses.

(E) Photostimulation of the interneuron four times with identical power (190 mW) induced the same number of APs every time.

(F) Paired recording of connected sGFP interneuron and layer 2/3 PC. Both cells are loaded with Alexa 594. Traces of inhibitory responses recorded in the PC (black traces) after one or two APs evoked in the sGFP interneuron (red traces) with 50 ms, +50 pA, and +120 pA current injection pulses, respectively. The interneuron was held at resting membrane potential in current-clamp and the PC was held in voltage-clamp at +40 mV.

(G) Inhibitory responses recorded in PC after one AP evoked in the connected sGFP interneuron by current injection (50 ms pulse, +50 pA) or by two-photon RuBi-Glutamate uncaging.

(H) Effect of RuBi-Glutamate on synaptic transmission between sGFP interneuron and PC. (H₁) Responses recorded in the PC, in response to 50 ms, 100 pA current injection pulses in the sGFP interneuron, before (left) and after (right) adding RuBi-Glutamate to the bath. (H₂) Average GABA current inhibition by RuBi-Glutamate ($47.3\% \pm 10.8\%$, $n = 7$).

(I) Example of a weak connection between a sGFP interneuron and a PC (10.5 pA in average), detectable by evoking a burst of APs in the sGFP interneuron.

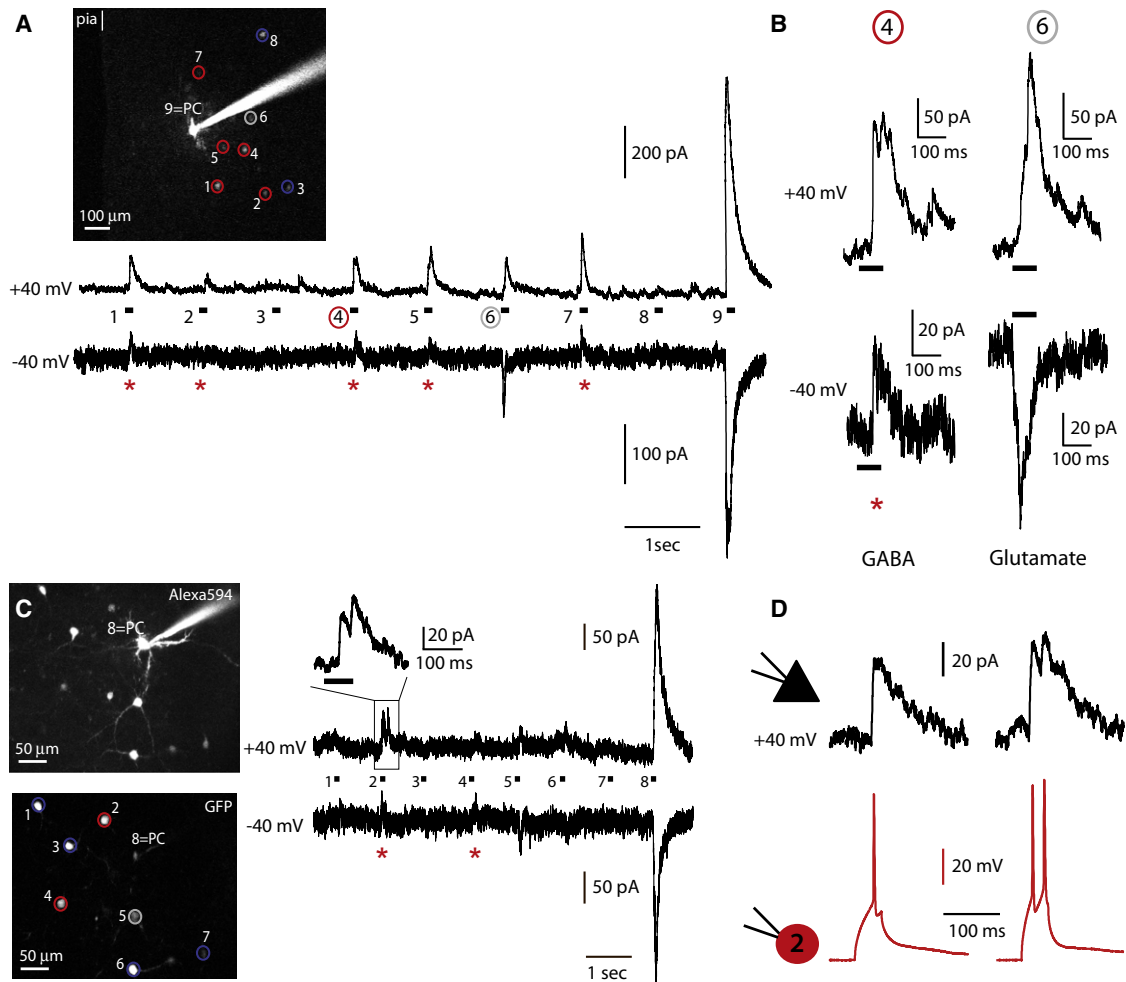


Figure 2. Detection of Inhibitory Connections

(A) Layer 2/3 field with a recorded PC (PC, #9), filled with Alexa 594, and 8 different sGFP interneurons (#1 to 8). Circles indicate connected interneurons (red), unconnected ones (blue) or false-positive responses (gray). Below are voltage-clamp recordings of evoked responses in PC when sequentially stimulating each sGFP interneuron; the PC was either clamped at +40 mV (top trace) or at -40 mV (bottom trace). Red stars indicate traces corresponding to connected GFP cells and circled numbers are the ones expanded in (B).

(B) Responses recorded in PC at +40 mV (top traces) or -40 mV (bottom traces) for a connected interneuron (#4) or a false positive cell (#6). A connected interneuron (#4) induces an inhibitory response (GABA), outward at +40 mV or -40 mV. A false positive (#6) is an excitatory response, outward at +40 mV but inward at -40 mV (Glutamate).

(C) Another layer 2/3 field with a recorded PC, and 7 sGFP interneurons. Recordings and color code as in (A). The response evoked by connected interneuron #2 is expanded.

(D) Electrophysiological confirmation that interneuron #2 and the PC were connected. Current-clamp recording of connected interneuron #2 (red) and responses evoked in the PC (black) following one or two APs. The interneuron was held at resting membrane potential in current-clamp and the PC was held in voltage-clamp at +40 mV. The IPSC had a latency of 1.29 ± 0.20 ms ($n = 6$) and an amplitude of 31.3 ± 11.5 pA ($n = 6$), matching our previous characterization of sGFP-PCs connections (Table 2).

See also Figures S1 and S2.

significantly contaminated by the spurious stimulation of neighboring ones.

Therefore, on a cell-by-cell basis, the switch from +40 mV to -40 mV allowed us to immediately discriminate false from true positives and detect monosynaptic inhibitory connections from the stimulated sGFP cell. Within a typical experiment, we first voltage-clamped at +40 mV, we measured all detectable synaptic connections and, at then, switching at -40 mV, we distinguished inhibitory connections from excitatory ones

(Figure 2B). Also, to test whether RuBi-Glutamate uncaging was efficient, in each experiment we also optically stimulated the patched PCs at the end of each photostimulation protocol (Figures 2A and 2C, last response).

Although our control experiments indicated that the stimulated sGFP cells that generated responses with GABAergic reversal potential in the PC were connected to it, we still decided to independently confirm the accuracy of the method with a different technique. For this, we used dual whole-cell recordings from

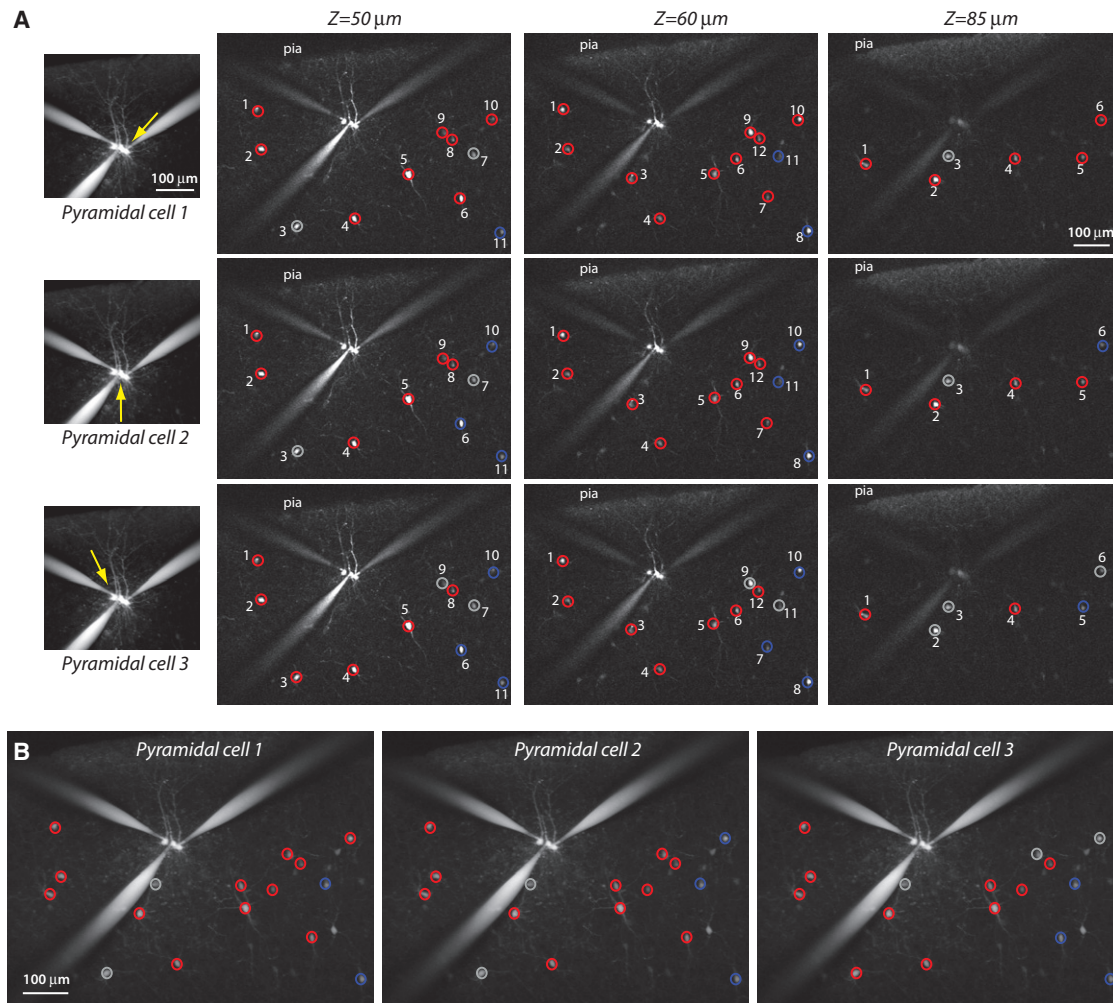


Figure 3. Two-Photon Mapping of Inhibitory Inputs in Three Dimensions

(A) Left: Images of PCs filled with Alexa 594; the position of each PC is indicated by a yellow arrow. Right: Images of sGFP interneurons, at different depths (50, 60, and 85 μm) (vertically) for the three different PCs (horizontally). On each image, all the stimulated sGFP cells are indicated by a number and the colored circles indicate connected interneurons (red circles), unconnected ones (blue circles), or false-positive responses (gray circles) to the appropriate PC.

(B) Projected Z stack of the field representing the summary of all connections found for each recorded PC within the whole field. Some cells are stimulated on two different depths so represent only one cell on the summary. Note how in this slice, most of sGFP cells are connected to PCs.

sGFP neurons whom we predicted optically were connected to the PC. For this purpose, after testing the inhibitory connections with photostimulation, we patched putative presynaptic connected sGFP cells (i.e., those whose evoked responses did not switch at -40 mV) with another electrode and stimulated them by injecting depolarizing current pulses, while simultaneously recording responses in the PC (Figures 2C and 2D). Indeed, in 11 out of 12 cases, APs elicited in the putatively connected sGFP cell triggered inhibitory responses in the postsynaptic PC (Figure 2D). These IPSCs had short latencies, indicating a monosynaptic transmission (1.29 ± 0.20 ms, $n = 6$) and an average amplitude of 31.3 ± 11.5 pA ($n = 6$), these values being consistent with those measured from control paired recordings (Table 2). This demonstrated that two-photon RuBi-Glutamate uncaging was an accurate method to identify inhibitory connections.

Dense Local Inhibitory Innervation of Pyramidal Cells

We then proceeded to use this optical method to map connections from upper layers sGFP interneurons to layer 2/3 PCs. In a typical experiment, we recorded 2 or 3 PCs simultaneously while sequentially photostimulating every sGFP cell in the field of view (Figure 3). To increase the number of tested interneurons, we took advantage of the optical sectioning of two-photon excitation and stimulated interneurons located at different depths, stimulating 10 to 46 sGFP cells per experiment (Figures 3A and 3B; average 19.7 ± 0.9 interneurons, $n = 27$ fields). In all, we recorded 20 simultaneous maps of pairs and 7 of triplets of PCs, for a total of 61 maps, testing 1245 putative presynaptic neurons. In these maps we classified each tested sGFP cell as being either (1) connected, evoking inhibitory responses (red), (2) unconnected, evoking no response (blue), or (3) false positive, evoking an excitatory response (gray) (Figure 3; see above). Over

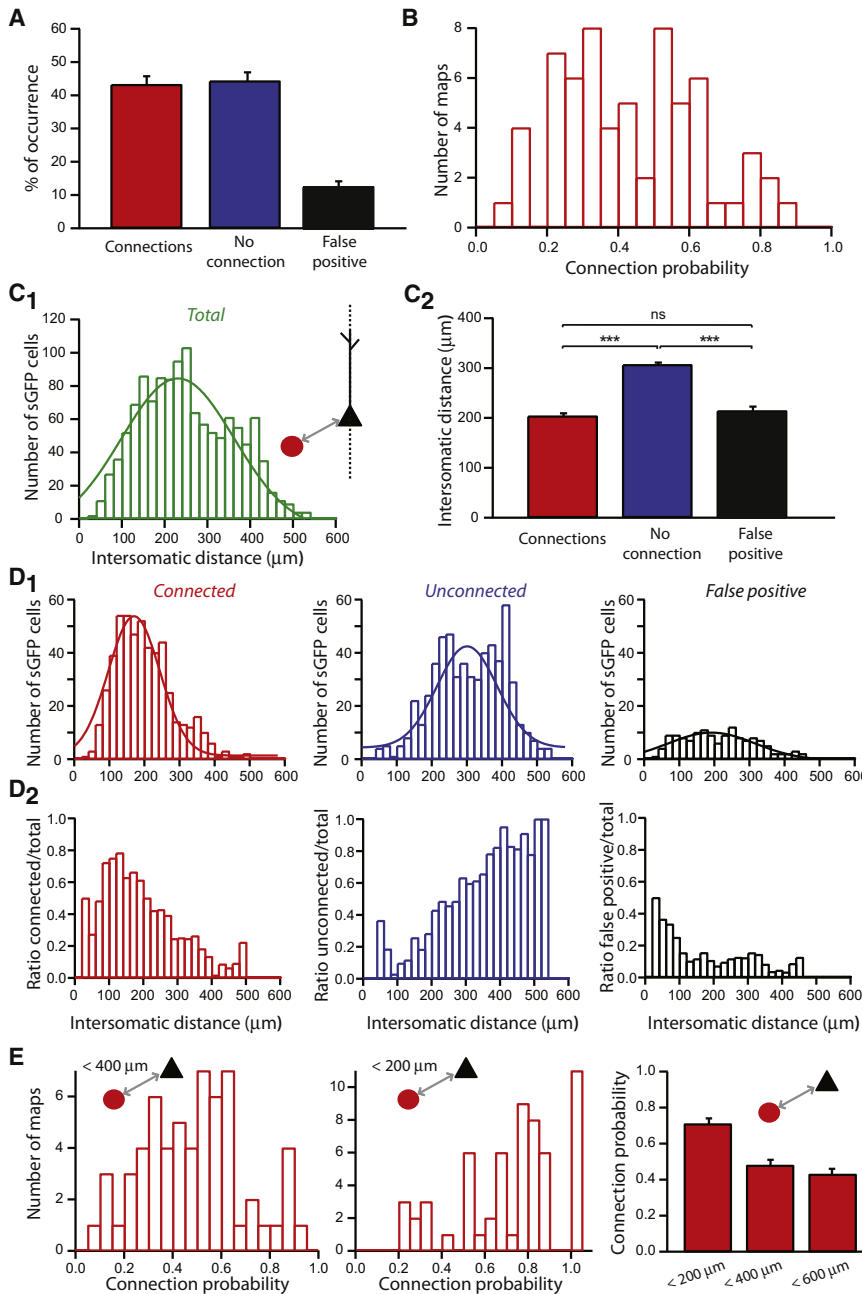


Figure 4. Dense Innervation and Distance-Dependence of Connectivity

(A) Proportions of connected (red) and unconnected interneurons (blue) and false positive responses (black) within all tested sGFP interneurons.

(B) Connection probability for all stimulated interneurons in all maps.

(C₁) Distribution of intersomatic distances for all the sGFP interneurons tested and schematic representation of the measurement. The peak was centered on $230.83 \pm 5.3 \mu\text{m}$ ($n = 1245$). (C₂) Averaged intersomatic distances between PCs and connected (red) and unconnected (blue) interneurons and false-positive cells (black). Connected interneurons were significantly ($p < 0.0001$, Mann-Whitney) closer to the PC than unconnected ones but not significantly different than false-positive cells.

(D₁) Distributions of the intersomatic distances between PCs and connected (red) and unconnected interneurons (blue) and false positives (black). Peaks were centered on $170.54 \pm 4.55 \mu\text{m}$ ($n = 520$) for connected interneurons, $300.63 \pm 5.02 \mu\text{m}$ ($n = 584$) for unconnected interneurons and $192.15 \pm 14.80 \mu\text{m}$ ($n = 141$) for false positives. (D₂) Distributions of ratios of intersomatic distances between PCs and connected (red) and unconnected interneurons (blue) and false positives (black), normalized over the total number of stimulated interneurons.

(E) Distribution and averages of the connection probabilities for stimulated interneurons within a radius of $400 \mu\text{m}$ or $200 \mu\text{m}$ from the PCs. *** $p < 0.0001$.

See also Figure S3.

somatic distances between stimulated sGFP cells and recorded PCs. sGFP neurons were located at distances ranging from ~ 50 to $550 \mu\text{m}$ from the PCs (Figure 4C₁). Connected interneurons were significantly closer to recorded PCs than unconnected ones (mean distance for connected $203.9 \pm 5.5 \mu\text{m}$, $n = 520$ versus $306.9 \pm 4.1 \mu\text{m}$, $n = 584$ for unconnected; $p < 0.0001$, Mann-Whitney; Figures 4C₂ and 4D₁). False-positive responses were located closer to the PCs as well (mean $214.2 \pm 8.6 \mu\text{m}$, $n = 141$),

consistent with the hypothesis that they might be mainly due to direct stimulation of the recorded PC. To better illustrate the difference in distributions between connected and unconnected neurons, we plotted the histograms of the ratios of connected, unconnected, or false-positive responses over the total number of stimulated interneurons (Figure 4D₂). The peak of the distribution of the ratio of connected over total interneurons peaked at less than $200 \mu\text{m}$, whereas the unconnected interneurons peaked beyond $400 \mu\text{m}$, and the false positives at less than $100 \mu\text{m}$.

These distributions demonstrated that the probability for interneurons to be connected decreases with intersomatic

all 61 maps, $43.2\% \pm 2.5\%$ of stimulated sGFP interneurons were connected to the recorded PCs, while $44.3\% \pm 2.6\%$ were unconnected and the remaining $12.5\% \pm 1.6\%$ were false positive responses (Figure 4A). Analyzing each map independently, we calculated the connection probability, i.e., the number of connected sGFP cells over the total number of stimulated sGFP cells, for each field tested. This revealed that the range of the connection probability was very large, from 0.1 to 0.9 (Figure 4B).

We analyzed the spatial structure of the connected cells to determine whether there was a distance dependence of the inhibitory connectivity. For this purpose, we measured the inter-

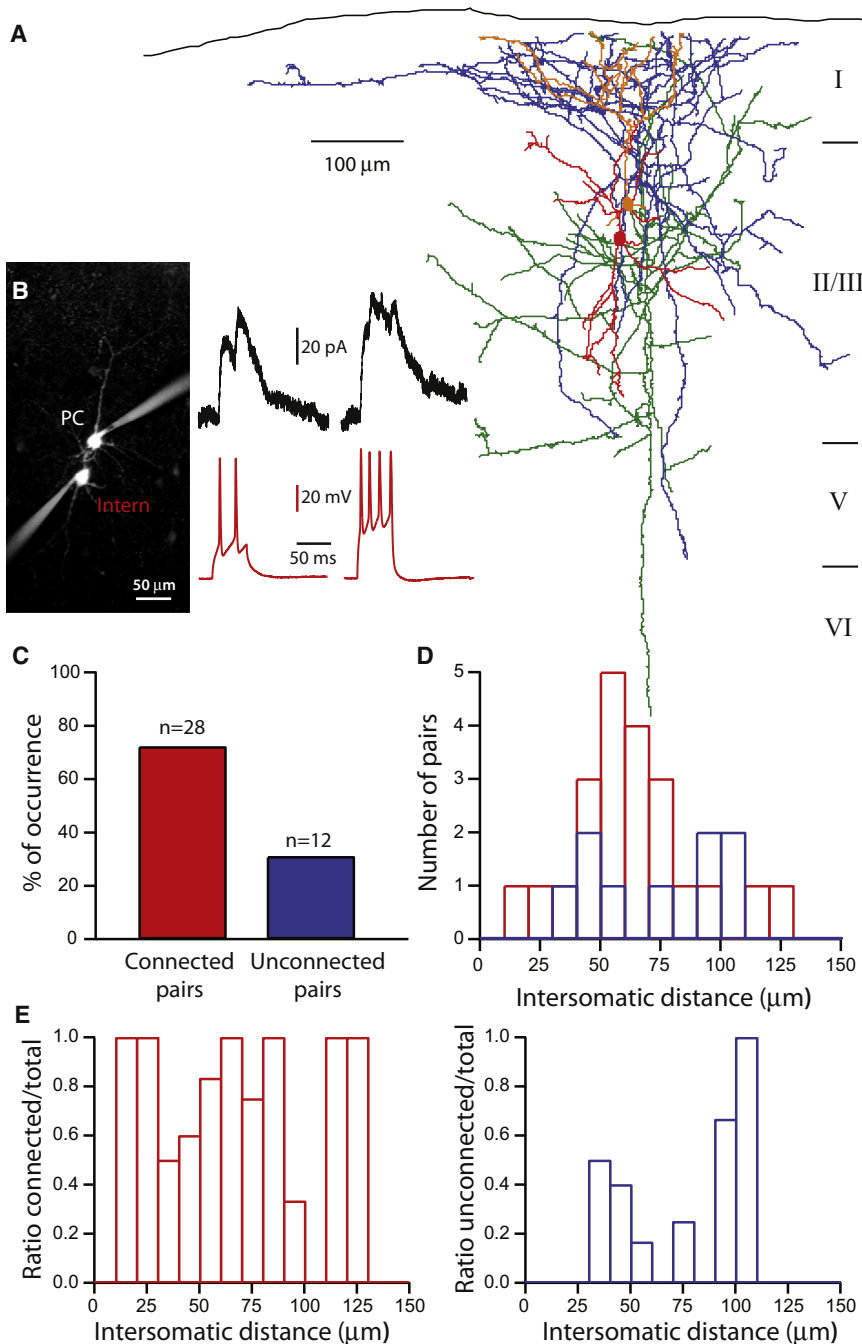


Figure 5. Paired Recordings Confirm Local Dense Inhibitory Innervation

(A) Reconstruction of a connected pair of sGFP interneuron and PC after biocytin labeling. Pia is indicated in black at the top. The dendrites of the interneuron are red and axon in blue and dendrites of PC are orange, with axon in green. Notice the large overlapping area of the interneuron axon and the PC dendrites.

(B) Image of the connected pair showed in (A), the cells are filled with Alexa 594 and electrophysiological recordings of the connection: inhibitory responses recorded in PC (black traces) after two (50 ms, 150 pA) or a burst (50 ms, 300 pA) of APs evoked in the sGFP interneuron (red traces).

(C) Proportion of connected and unconnected pairs from dual recordings. Within 40 patched pairs, 70% (n = 28) were connected and 30% (n = 12) were not.

(D) Intersomatic distances for connected (red, average: $61.90 \pm 5.25 \mu\text{m}$, n = 23) or unconnected (blue, $73.6 \pm 9.4 \mu\text{m}$, n = 9) pairs. There is no significant difference in the intersomatic distances for connected or unconnected sGFP-PC pairs.

(E) Ratios of connected pairs (red) and unconnected pairs (blue) over the total number of pairs.

Confirmation of Dense Connectivity with Paired Recordings

We were surprised by the high local sGFP cell-PC connectivity revealed by our optical mapping technique and therefore aimed to confirm this finding with paired recordings (Figure 5). For this purpose, we patched pairs of sGFP cells and PCs, selected randomly from a local population, to identify connected ones. From 40 pairs, 70% (n = 28) were monosynaptically connected and 30% (n = 12) were unconnected (Figures 5A–5C). The morphology of one reconstructed connected sGFP cell-PC pair showed a typical Martinotti morphology, with an axonal projection of a Martinotti cell toward the pia (Figure 5A). This large axon and the PC dendrites overlapped, with many potential connection sites. There was no significant difference between the distribution of intersomatic

distances, peaking at less than $200 \mu\text{m}$ and becoming negligible beyond $400 \mu\text{m}$ (Figures 4D₁ and 4D₂). To better explore this, we plotted the connection probability within a 400 or $200 \mu\text{m}$ radius from the PCs (Figure 4E) and observed that the connection probability was 0.48 ± 0.03 (n = 61) within $400 \mu\text{m}$, but increased to 0.71 ± 0.03 (n = 61) within $200 \mu\text{m}$. Thus, the probability of connections from sGFP interneurons to PCs within a local circuit (< $200 \mu\text{m}$) can be very high. Indeed, if one discards false positive responses, in 11/61 maps, every single tested interneuron in the near vicinity (< $200 \mu\text{m}$) of a PC were connected to it (Figures 3 and 4E).

distances for connected ($61.9 \pm 5.3 \mu\text{m}$, n = 23) or unconnected ($73.6 \pm 9.4 \mu\text{m}$, n = 9) sGFP-PC pairs (p = 0.26, t test; Figure 5D). Intersomatic distances between sGFP cells and PCs were within $150 \mu\text{m}$ (average of 65.0 ± 4.5 , n = 32) and the probability of being connected was homogeneously high from 0 to $150 \mu\text{m}$ (Figure 5E). In fact, the average connection probability observed for these recorded pairs (0.7) was similar to the probability observed in RuBi-Glutamate mapping experiments within a $200 \mu\text{m}$ radius from the PC (0.71 ± 0.03 , n = 61). In addition, analyzing the connection probability within $150 \mu\text{m}$ intersomatic

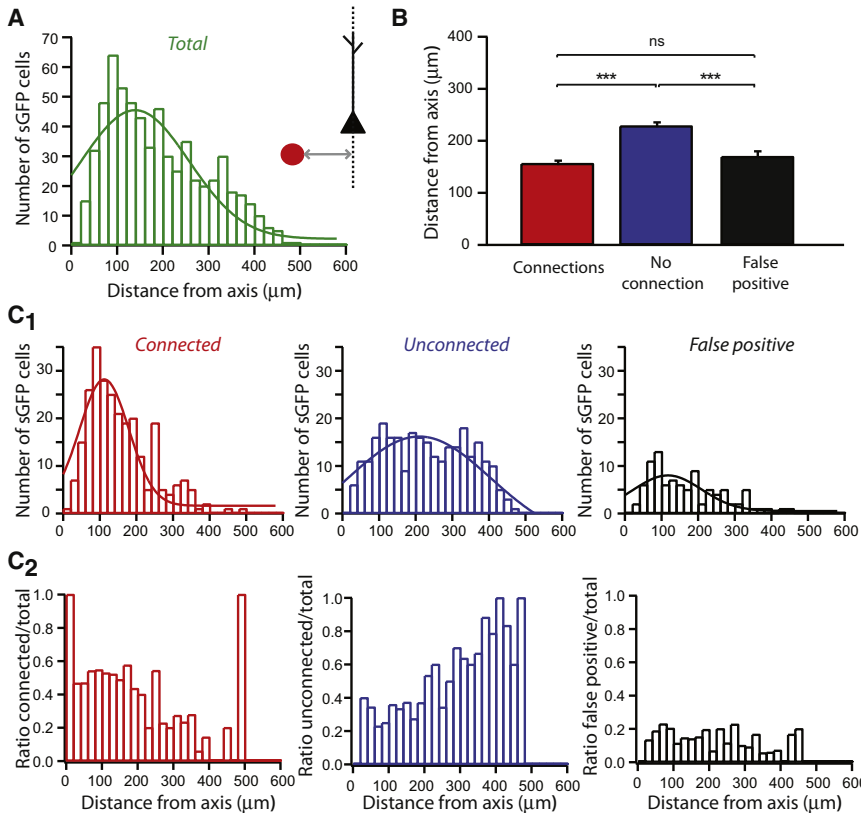


Figure 6. Analysis of Columnar Connectivity

(A) Distribution of distances from the PC vertical axis to all sGFP cells tested and schematic representation of the measurement. The peak was centered on $144.3 \pm 10.3 \mu\text{m}$ ($n = 1245$).

(B) Average distances from PC axis to connected (red) and unconnected interneurons (blue) and false positives (black). Connected interneurons were significantly ($p < 0.0001$, Mann-Whitney) closer to the PC vertical axis than unconnected interneurons but similar to false positives.

(C₁) Distribution of distances from PC axis to connected (red) and unconnected interneurons (blue) and false positives (black). Peaks were centered on $114.10 \pm 5.53 \mu\text{m}$ ($n = 520$) for connected interneurons, 219.65 ± 12.00 ($n = 584$) for unconnected interneurons and 80.86 ± 5.12 ($n = 141$) for false positives. (C₂) Distributions of ratios of connected (red), unconnected (blue), and false positives (black) interneurons, depending on the distances from the PC axis. *** $p < 0.0001$.

distances from the optical mapping experiments, to match with the distances considered with the paired recordings, also demonstrated a similar connection probability (0.73 ± 0.04 , $n = 61$).

Altogether, these results from the optical mapping and paired recording experiments indicate a dense inhibitory connectivity from the somatostatin-expressing interneurons within local circuits ($<200 \mu\text{m}$ distance from the PC).

Columnar and Depth Analysis of Connectivity

Intracortical connectivity has long been assumed to be vertically organized (“chains” or “columns” [Lorente de N6, 1949; Mountcastle, 1982]), and this columnar organization has been observed in the frontal cortex as well (Isseroff et al., 1984). Therefore, we reanalyzed the optical mapping data, measuring the distances between the soma of the sGFP interneurons and a line through the recorded PCs, perpendicular to the pial surface (Figure 6A); this line would correspond to the axis of a hypothetical column. In this analysis, we observed a narrower distribution of the distances of connected interneurons, on average located at $\sim 100 \mu\text{m}$ from a putative columnar axis (Figures 6B and 6C). Unconnected cells were located on average at $>200 \mu\text{m}$ from this axis, displaying a broad distribution of distances. False positives showed a peak centered at $<100 \mu\text{m}$ of from the axis (Figure 6C). This analysis showed therefore that sGFP cells located within the same “column” of the considered PCs are more likely to contact and modulate them. This is consistent with the anatomy of somatostatin-expressing interneurons (Figure 5A), which have vertical axonal arborizations projecting toward the

pia and with the vertical organization of the disynaptic inhibition mediated by these interneurons that have been previously described (Silberberg and Markram, 2007). These observations also reinforce the idea of the existence of vertical functional connectivity within the cortex.

Finally, since our experiments were performed on brain slices, we explored the depth dependency of the connectivity but did not observe any correlations between the inhibitory connectivity and the depth of the interneurons or PCs (Figure S3 and Supplemental Information).

Lack of Specific Subnetworks

Our results indicated that the inhibitory innervation of PCs can be quite dense locally, which would imply that the connectivity from sGFP cells to local PCs is not selective and that they do not form specific subnetworks. To examine this more closely, we exploited the fact that, we were able to simultaneously record and build input maps from several postsynaptic PCs (Figures 3 and 7A). This enabled us to test whether sGFP input maps of different PCs were correlated or not. Specifically, we compared inhibitory inputs to two or more PCs that were connected among themselves and thus belong to the same synaptic circuits with those to PCs that were not connected and might belong to different functional circuits. This type of analysis, comparing inputs maps from connected or unconnected postsynaptic targets, has been previously used in several studies to examine the selectivity in the synaptic connectivity of neurons (Kampa et al., 2006; Yoshimura et al., 2005). For this purpose, we recorded 20 simultaneous maps of pairs and 7 of triplets of PCs. Within these maps, we compared maps obtained from pairs of unconnected PCs ($n = 33$) with those from connected ones ($n = 8$). Connections between PCs had EPSCs with average amplitudes of $15.70 \pm 2.36 \text{ pA}$ and latencies of $3.33 \pm 0.42 \text{ ms}$

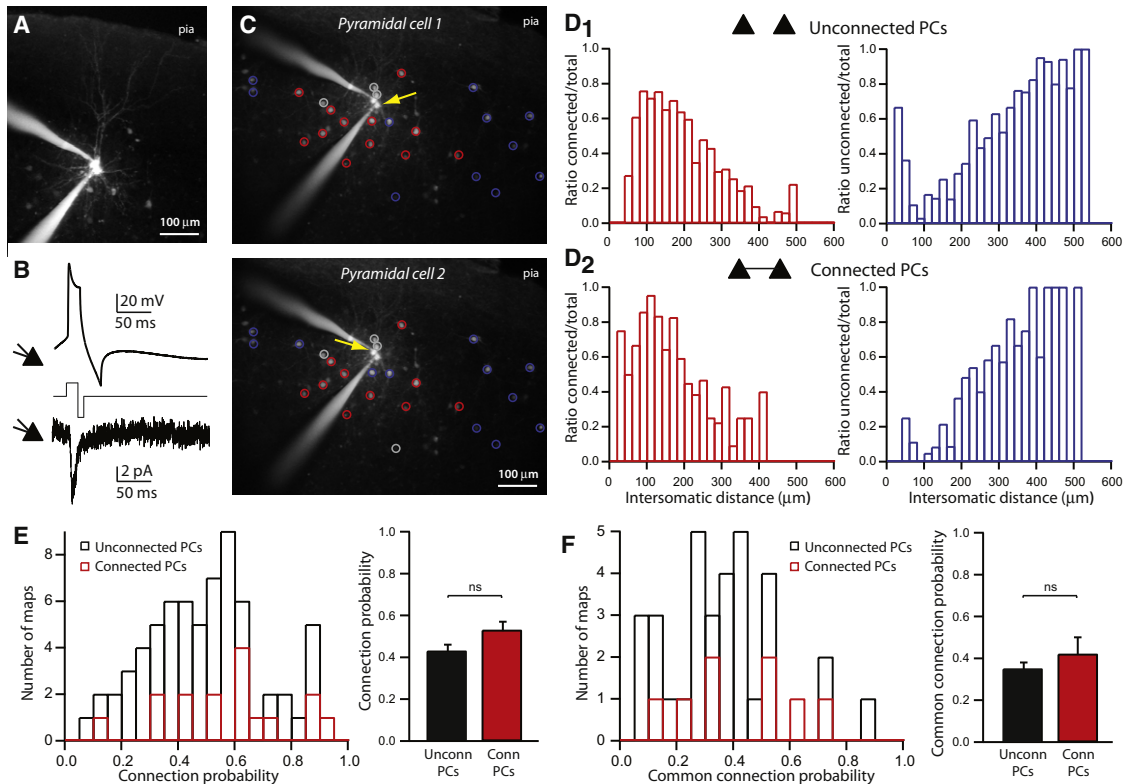


Figure 7. Lack of Specific Subnetworks

(A) Pair of connected PCs filled with Alexa 594.

(B) Example of a recording of a connected PC pair (with Cs-based internal; see Supplemental Information).

(C) Maps of inhibitory inputs onto two connected PCs. Colored circles indicate connected interneurons (red), unconnected ones (blue), or false-positive responses (gray). Yellow arrows indicate position of the PC.

(D) Distributions of ratios of connected (red) and unconnected interneurons (blue) over the total number of stimulated interneurons for unconnected PCs (D₁) or connected PCs (D₂). These distributions were not significantly different between connected and unconnected PCs, either for connected ($p = 0.48$, Wilcoxon paired test) or unconnected interneurons ($p = 0.21$).

(E) Distribution and averages of the probability of inhibitory connections for pairs of PCs, for unconnected PCs (black) or connected PCs (red). There was no significant difference ($p = 0.07$, Mann-Whitney test) in connection probability between connected and unconnected PCs.

(F) Distribution and averages of the probability of receiving common inhibitory inputs for pairs of PCs, for unconnected PCs (black trace) or connected PCs (red trace). There was no significant difference ($p = 0.36$, Mann-Whitney test) in common connection probability between connected and unconnected PCs.

($n = 8$; Figure 7B and Table 3). All PCs, connected or not, were close to each other ($<50 \mu\text{m}$).

We did not detect any obvious difference between maps of unconnected PCs (Figure 3) or connected PCs (Figure 7C). To examine this more carefully we analyzed these maps quantitatively (Figures 7D–7F). Both types of maps had similar numbers of stimulated sGFP cells (for unconnected PCs: range 11–46; average = 19.6 ± 1.3 , $n = 33$ versus for connected PCs: range 15–30; average = 21.9 ± 2.2 , $n = 8$, $p = 0.23$, t test) and a similar connection probability from sGFP cells (0.43 ± 0.03 , $n = 66$ for unconnected PCs versus 0.53 ± 0.04 , $n = 16$ for connected PCs; $p = 0.07$, Mann-Whitney test; Figure 7E). We compared the spatial distribution of connections between both types of maps, by plotting, for each distance, the ratios of connected or unconnected interneurons over the total number of stimulated sGFP cells (Figures 7D₁ and 7D₂). A Wilcoxon matched-paired test revealed that the distributions of connected or unconnected sGFP cells were similar between

maps of connected or unconnected PCs ($p = 0.48$ for connected GFP cell distributions and 0.21 for unconnected ones). Finally, we calculated the overall probability of receiving common sGFP inputs for pairs of PCs and tested whether this differed between connected or unconnected PCs, as one would expect if sGFP cells formed specific subnetworks with PCs. For this analysis, we only considered sGFP cells within $400 \mu\text{m}$ from the PCs, because the probability for these interneurons to be connected becomes negligible beyond $400 \mu\text{m}$ (Figure 4C). We defined this probability as the number of common inputs divided by the total number of stimulated interneurons and observed that it was similar between connected (0.42 ± 0.08 , $n = 8$) and unconnected PCs (0.35 ± 0.03 , $n = 33$; $p = 0.36$, Mann-Whitney; Figure 7F). This indicates that synaptically connected PCs, which are part of the same synaptic circuits, receive as many common sGFP inputs as unconnected PCs. These results overall suggest that sGFP cells appear to connect with PCs in a similar fashion, without

Table 3. Characteristics of Synaptic Transmission between Two Layer 2/3 Pyramidal Cells

	All Pairs (n = 13)	P11–P16 (n = 8)	P20–P41 (n = 5)
Latency (ms)	3.12 ± 0.30	3.33 ± 0.42	2.78 ± 0.42
Rise time (ms)	5.15 ± 0.66	5.15 ± 0.69	5.14 ± 1.59
Amplitude (pA)	15.17 ± 3.16	15.70 ± 2.36	14.31 ± 8.51
Rate of rise (pA/ms)	3.74 ± 1.06	3.31 ± 0.53	4.43 ± 3.00
Failure rate (%)	17.20 ± 4.53	20.01 ± 5.66	13.10 ± 8.76

discriminating whether these PCs are connected or not and therefore do not form specific subnetworks.

Dense and Unspecific Inhibitory Connectivity in Mature Neocortex

We performed our initial mapping experiments with young animals (P11–P16), relatively early in the development of these circuits. It was therefore possible that the dense and unspecific organization of inhibitory circuit would be a transitory developmental state and that similar mapping in older animals could yield sparser, perhaps more specific, functional maps. To test this hypothesis, we performed optical mapping experiments with older animals, in a range of developmental stages from P11 to P41, which encompass the normal maturation of mouse neocortical circuits through critical periods and into adulthood (Fagiolini and Hensch, 2000). We observed that the connection probability was similar throughout the range of ages examined ($p > 0.05$, one-way ANOVA): P11 to P12 (0.49 ± 0.04 , $n = 26$), P13 to P14 (0.38 ± 0.03 , $n = 28$), P15 to P17 (0.47 ± 0.06 , $n = 10$), P18 to P20 (0.56 ± 0.06 , $n = 11$), P22 to P23 (0.55 ± 0.05 , $n = 10$), P26 to P30 (0.52 ± 0.12 , $n = 4$), P34 to P35 (0.56 ± 0.04 , $n = 8$), and P36 to P41 (0.54 ± 0.05 , $n = 7$) (Figure 8A). It should be noted that there was a small significant decrease in connection probability at P13–P14 ($p = 0.04$, compared to P11–P12; Mann-Whitney), which could indicate a potential remodeling of the connectivity in the cortical circuits at the opening eyes stage of the development.

The proportions of connected, unconnected interneurons and false positive were not significantly different for young (P11–P16) versus mature (P20–P41). The mature mapping revealed $55.8\% \pm 2.4\%$ of connected sGFP cells (versus $43.2\% \pm 2.5\%$ for young, $p = 0.65$, *t* test), $39.0\% \pm 2.5\%$ of unconnected sGFP cells (versus $44.3\% \pm 2.6\%$ for young, $p = 0.85$, *t* test) and $5.3\% \pm 1.0\%$ of false positives (versus $12.5\% \pm 1.6\%$ for young animals, $p = 0.67$, *t* test). The spatial organization of the mature maps indicated that the distributions of the intersomatic distances for all the stimulated sGFP cells were similar to the one observed for young maps (Figure 8B). Sampled sGFP neurons were located at distance ranging from ~ 50 to $500 \mu\text{m}$ from the PCs (Figure 8B). Connected interneurons were significantly closer to the recorded PCs than unconnected ones (mean distance for connected $191.9 \pm 4.3 \mu\text{m}$, $n = 447$ versus $278.3 \pm 5.8 \mu\text{m}$, $n = 315$ for unconnected; $p < 0.0001$, Mann-Whitney; Figure 8B). False-positive responses were located close to the PCs as well (mean $141.1 \pm 14.1 \mu\text{m}$, $n = 45$). The mean intersomatic distances observed for mature animals were not significantly different

than the ones observed for younger ones. Interestingly, both young and mature animals also showed a similar proportion of fully connected maps locally (within $200 \mu\text{m}$): 11/61 maps from young animals and 5/34 from mature ones revealed that every nearby interneurons was connected to the sampled PC.

Finally, we tested whether the organization of inhibitory inputs was more specific for mature animals. We compared the inhibitory input maps of connected PCs (Table 3) versus unconnected PCs. Similarly to young animal maps, we did not detect any obvious difference between maps of unconnected or connected PCs for mature animals. Maps at both ages had similar numbers of stimulated sGFP cells (for unconnected PCs: 19.5 ± 3.1 , $n = 10$ versus for connected PCs: 16.5 ± 3.4 , $n = 5$, $p = 0.56$, *t* test). The spatial distribution of connections, represented by the ratios of connected interneurons over the total number of stimulated sGFP cells for each distance (Figures 8C₁ and 8C₂), was not significantly different for unconnected PCs and connected PCs ($p = 0.24$, Wilcoxon paired test). Unconnected and connected PCs also had a similar probability to obtain connections from sGFP cells (connection probability for unconnected PCs = 0.58 ± 0.04 , $n = 20$ versus 0.60 ± 0.04 , $n = 10$ for connected PCs; $p = 0.83$, Mann-Whitney test; Figure 8D). Finally, we tested the specificity of the inhibitory connections for mature animals by calculating the overall probability of receiving common sGFP inputs for pairs of PCs (common inputs divided by the total number of stimulated interneurons) and tested whether this differed between connected or unconnected PCs. This probability was similar between connected (0.46 ± 0.02 , $n = 5$) and unconnected PCs (0.44 ± 0.05 , $n = 10$; $p = 0.67$, Mann-Whitney; Figure 8E). This indicates that, similarly to young animals, synaptically-connected PCs in mature animals receive as many common sGFP inputs as unconnected PCs. These results overall demonstrate that, from early developmental stages to mature stages, sGFP cells densely contact PCs, without discriminating whether these PCs are connected or not and therefore without forming any specific inhibitory subnetworks.

DISCUSSION

Optical Mapping of Connections with Single-Cell Resolution

In this study, we use an optical technique to map the connectivity between identified cell types in neocortical circuits, generating single-cell resolution maps of their synaptic circuits. By using RuBi-Glutamate, a caged glutamate compound that allows recording GABAergic inputs (Fino et al., 2009), and a line of transgenic mice where somatostatin-expressing neurons are labeled with GFP (Oliva et al., 2000), we adapted two-photon photostimulation (Nikolenko et al., 2007), which itself developed out of previous one-photon photostimulation efforts (Callaway and Katz, 1993; Farber and Grinvald, 1983), to map inhibitory connections. Here, we performed control experiments showing that the photostimulation and mapping are reliable. We can differentiate between direct stimulation of the recorded pyramidal cells (false positives) and true inhibitory connections and do not find clear evidence of unspecific activation of other inhibitory neurons not targeted by the laser. Using post hoc paired recordings, we confirm that at least 90% of the neurons which we predicted

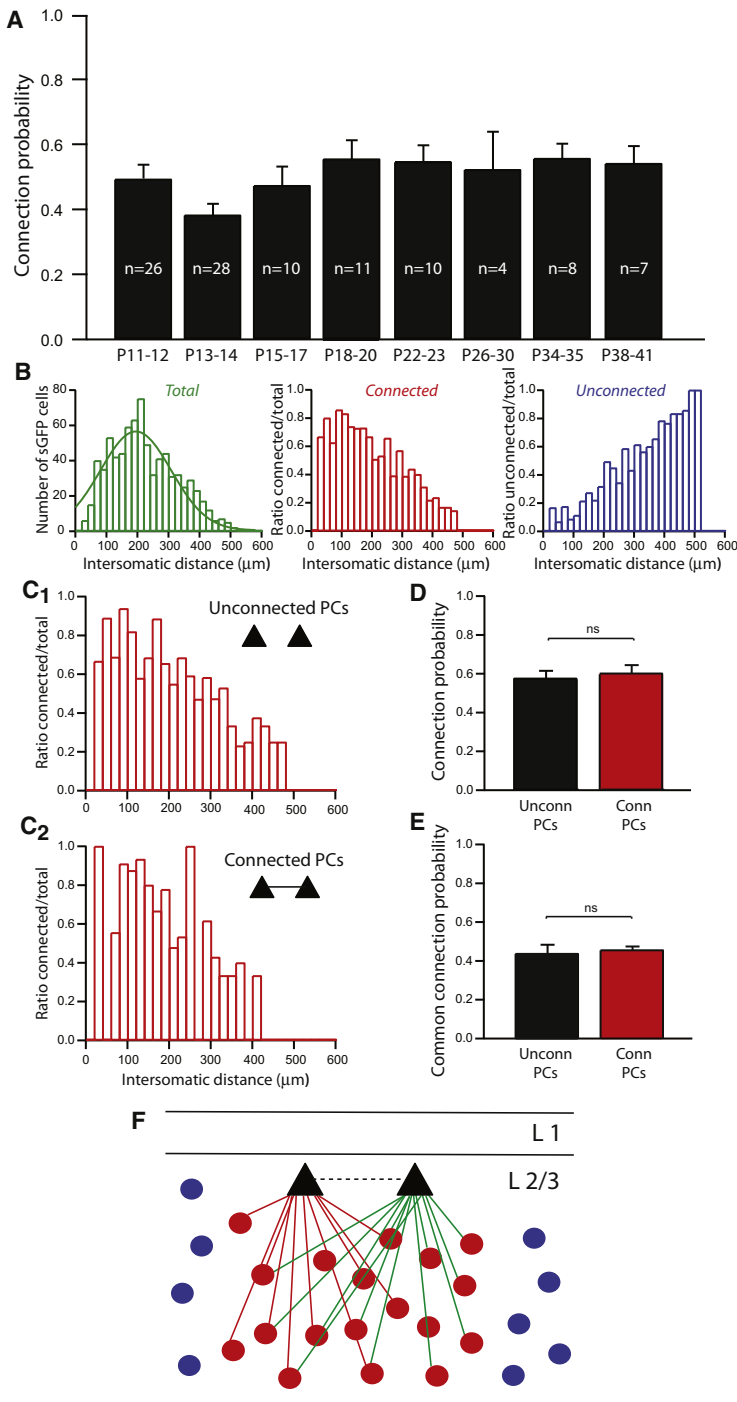


Figure 8. Dense Inhibitory Innervation across Different Developmental Stages

(A) Connection probability from sGFP cells to PCs at different developmental stages. The inhibitory connection probability is not statistically different throughout the whole range of ages ($p < 0.05$, one-way ANOVA).

(B) Intersomatic distances for older animals (P20 to P41) for all stimulated sGFP cells; the peak is centered on 194.79 ± 5.74 ($n = 787$). Ratios of connected (red) or unconnected (blue) sGFP cells over the total number of stimulated sGFP cells, as a function of intersomatic distances between sGFP cells and PCs, for older animals (P20–P41).

(C₁ and C₂) Ratios of connected interneurons over total number of stimulated interneurons for unconnected PCs (C₁) or connected PCs (C₂) (P20–P41). There was no significant difference ($p = 0.24$, Wilcoxon paired test) between connected and unconnected PCs for connected interneurons spatial organization.

(D) Distribution of the probability of inhibitory connections for pairs of PCs (P20–P41), for unconnected PCs (black) or connected PCs (red). There was no significant difference ($p = 0.83$, Mann-Whitney test) of connection probability for unconnected or connected PCs. (E) Distribution of the probability of receiving common inhibitory inputs for pairs of PCs (P20–P41), for unconnected PCs (black trace) or connected PCs (red trace). The common connection probability was not significantly different ($p = 0.67$, Mann-Whitney test) for unconnected or connected PCs.

(F) Hypothetical circuit model that could underlie our results: a dense connectivity of inhibitory inputs from sGFP interneurons where every interneuron is connected to each neighboring PC. Within a local region, the connectivity could be complete. Dashed line between the two PCs illustrates that the same model applies for connected or unconnected PCs.

mate or optogenetics, is limited to a coarse-grained mapping of laminar projections, which, while valuable, do not reveal the true nature of the connectivity matrix present in the microcircuits (Otsuka and Kawaguchi, 2009; Thomson and Lamy, 2007; Xu and Callaway, 2009; Yoshimura and Callaway, 2005). In addition, two-photon photostimulation can be performed through highly scattering media so circuit mapping can be carried out in three dimensions (Figure 3; Nikolenko et al., 2007). Also, two-photon mapping is performed with living tissues, and because it uses a functional assay for connectivity, it enables the mapping of functional variables and of the actual synaptic matrix of local synaptic weight of a neuron (Nikolenko et al., 2007). The method is fast, since one can test up to 500 neurons in 10 min (Nikolenko et al., 2007). One can also map changes in the connectivity map so it becomes possible to examine online the role of modulators or of plasticity-inducing

paradigms on a given circuit (Nikolenko et al., 2007). Finally, to quantify the specificity of a circuit one essentially needs to know the number of connected neurons (the numerator), divided by the number of total potentially connected neurons (the denominator). While other techniques can reveal connected neurons, they do not sample every possible connected cell, something that is possible with our technique, which can therefore provide the denominator of the equation.

were connected are indeed connected. This optical mapping technique is therefore accurate in correctly predicting inhibitory connections.

One key advantage of two-photon photostimulation is that it has single-cell resolution. This appears essential for examining the actual connectivity patterns in the central nervous system, built out of many cell types, which are often intermixed. Without single-cell resolution, photostimulation, either with caged glutamate or optogenetics, is limited to a course-grained mapping of laminar projections, which, while valuable, do not reveal the true nature of the connectivity matrix present in the microcircuits (Otsuka and Kawaguchi, 2009; Thomson and Lamy, 2007; Xu and Callaway, 2009; Yoshimura and Callaway, 2005). In addition, two-photon photostimulation can be performed through highly scattering media so circuit mapping can be carried out in three dimensions (Figure 3; Nikolenko et al., 2007). Also, two-photon mapping is performed with living tissues, and because it uses a functional assay for connectivity, it enables the mapping of functional variables and of the actual synaptic matrix of local synaptic weight of a neuron (Nikolenko et al., 2007). The method is fast, since one can test up to 500 neurons in 10 min (Nikolenko et al., 2007). One can also map changes in the connectivity map so it becomes possible to examine online the role of modulators or of plasticity-inducing

paradigms on a given circuit (Nikolenko et al., 2007). Finally, to quantify the specificity of a circuit one essentially needs to know the number of connected neurons (the numerator), divided by the number of total potentially connected neurons (the denominator). While other techniques can reveal connected neurons, they do not sample every possible connected cell, something that is possible with our technique, which can therefore provide the denominator of the equation.

Somatostatin Interneurons Densely Innervate Local Territories

We mapped the synaptic connections between one type of inhibitory interneurons onto an important class of cortical pyramidal neuron, layer 2/3 PCs. These PCs are among the most abundant of cortical cells, project to higher cortical areas, and are thought to play a fundamental role in the recurrent excitatory connectivity of the microcircuit (Mountcastle, 1998). In addition, layer 2/3 PCs integrate information from higher layers and project to layer 5 PCs, which are the output of the cortex.

We studied the inhibitory connections onto layer 2/3 PCs and focused on a population of somatostatin-positive cells. In a separate report, we analyzed in detail their morphologies and intrinsic electrophysiological properties in different cortical areas and concluded that they represented three different subtypes of neurons (McGarry et al., 2010). Nevertheless, in spite of this heterogeneity, in the upper layers of frontal cortex the majority of characterized GFP cells belonged to the Martinotti cell subtype (30/38 characterized neurons), so for the purpose of this current work, we assume that the sampled interneurons mostly represented Martinotti cells. As mentioned in the introduction, these interneurons contact dendrites of PCs and tightly regulate local synaptic integration, including the generation of dendritic spikes (Goldberg et al., 2004; Murayama et al., 2009). In addition, they could avoid circuit hyperexcitability since they are efficiently recruited by PC activity and mediate also a strong disinhibitory inhibition between PCs (Kozloski et al., 2001; Kapfer et al., 2007; Berger et al., 2009; Silberberg and Markram, 2007).

Here, we find a dense innervation of somatostatin-expressing interneurons onto PCs, which reinforces their potential central role in the network activity. The average probability of connections between sGFP interneurons and layer 2/3 PCs we observed (~50% within 400 μm and ~70% within 200 μm) is higher than previously described with double or triple patch-clamp recordings (~20% in layer 2/3 [Thomson and Lamy, 2007; Thomson and Morris, 2002; Thomson et al., 2002; Yoshimura and Callaway, 2005] and ~3% in layer 5 [Otsuka and Kawaguchi, 2009]) but agrees with the frequent occurrence of disinhibitory inhibition mediated by Martinotti cells (Berger et al., 2009; Silberberg and Markram, 2007).

We find a wide range of connection probability, from 0.1 to 1 within local circuits. Our method likely underestimates the connectivity, because of the slicing of neuronal processes, inefficiencies in the uncaging or in the photoactivation of the presynaptic neurons and also because of difficulty in detecting of small synaptic connections. Therefore, while one could explain a low connection probability by methodological constraints, maps with a high connection probability are particularly informative. In fact, in a substantial number of experiments, after discarding excitatory responses, locally, every single interneuron was connected to the sampled PCs (Figure 4E). These results are surprising, since they indicate that for some of the examined circuits, the local connectivity matrix could have been complete, meaning that every sGFP interneuron was locally connected to every PC. Moreover, this dense innervation is not just a transitory state during early phases of the cortical circuit maturation but also exists for older animals (Figure 8). This indicates that the dense inhibitory control of the somatostatin-expressing inter-

neurons must have a determinant role in the regulation of the cortical activity in the mature circuit.

Somatostatin Interneurons Lack Innervation Selectivity

Consistent with the promiscuous innervation of PCs, we find that sGFP cells do not form specific subnetworks, meaning that they connect to PCs similarly, regardless of whether these PCs are connected among themselves or not (Figures 7 and 8). A corollary of this conclusion is that layer 2/3 PCs themselves do not form subnetworks, at least based on their innervation by sGFP cells. Interestingly, somatostatin-positive cells are coupled together by gap junctions (Gibson et al., 1999; Peinado et al., 1993). Although we did not find evident electrotonic propagation of potentials or APs among sGFP neurons, the dense synaptic connectivity observed and the gap junctional coupling among these neurons agrees with the hypothesis that the entire sGFP population belongs to the same circuit.

Several studies have addressed the specificity of inhibitory connectivity in cortical microcircuits and most of them focused on the excitatory inputs onto interneurons (Otsuka and Kawaguchi, 2009; Xu and Callaway, 2009; Yoshimura and Callaway, 2005). The presence of specific inhibitory subnetworks have been tested with one-photon photostimulation experiments (Yoshimura and Callaway, 2005; Yoshimura et al., 2005) and paired recordings (Otsuka and Kawaguchi, 2009; Yoshimura and Callaway, 2005) and while some studies find specific subnetworks, others do not, with different result depending on the interneuron subtype (Otsuka and Kawaguchi, 2009; Thomson and Lamy, 2007; Yoshimura and Callaway, 2005). In agreement with Yoshimura and Callaway's paired recordings, in our data, taken from layer 2/3 frontal cortex, we do not find any clear evidence for specificity for the inhibitory connections from somatostatin-expressing interneurons to PCs.

Although one could interpret our results as demonstrating a complete lack of target selectivity, the fact that the maps are dense does not necessary imply that they are built by a random, nonspecific process. In fact, the complete connectivity that we observe appears in some cases deterministic, as if the circuit has been built to ensure that every interneuron is connected to every single local PC cell. We do not yet understand what the mechanisms underlying this dense connectivity are. It could be related to the relatively large axonal fields of Martinotti cells (McGarry et al., 2010), so one could perhaps expect this from the mere overall of these axons with the local dendritic fields of the local pyramidal neurons, following Peters' rule (Peters et al., 1976). At the same time, it is possible that more selective mechanisms could be at play to actively ensure a high local connectivity.

Implication for Cortical Modularity and Processing

The dense sampling of inputs implies a circuit model where the connectivity is maximized, perhaps even to the physical limit. In spite of the fact that our data was taken from brain slices, where many connections have been sectioned, we detect many instances where the connectivity is so dense that it approaches sampling every potential presynaptic input (Figure 8F). Since we randomly chose PCs and also found this dense innervation in pairs or triplets of simultaneously recorded PCs,

we interpret our results as indicating that, in principle, every interneuron might be connected to each local. It is unclear at this point if these results apply only to this population of interneurons in the frontal cortex or whether this very dense connectivity only exists for inhibitory interneurons or is a general feature of cortical connectivity. In any case, future studies need to be performed with other neuronal cell types to address whether our findings are generally applicable.

By densely innervating all local PCs, the subpopulation of interneurons that we have studied would affect their function in a global, nonselective manner. This occurs at all developmental stages tested. Although there have been several hypotheses that have suggested that inhibitory interneurons are involved in crafting specific responses in PCs, such as the generation of specific receptive fields (Runyan et al., 2010), our results are more in line of the idea that inhibition serves instead to locally control PCs, perhaps helping stabilize the transfer function of the circuit, but without a computational function “per se.” This would imply that they themselves are not involved in the generation of specific receptive field properties (Kerlin et al., 2010). Indeed, the different developmental origin of interneurons, late invaders of cortical territories (Xu et al., 2004) resonates well with an unspecific role, whereby they could arrive late and extend a “blanket of inhibition” throughout the circuit.

In finishing, one could reconsider the definition of cortical modules. While there is ample evidence for repetitive features in cortical design at the macroscopic level (“macrocolumns”; Grinvald et al., 1988; Hubel and Wiesel, 1977), the physical existence of cortical “minicolumns” (Mountcastle, 1982) has been doubted due to the lack of strong anatomical evidence (Crick and Asanuma, 1986). Our results provide a different viewpoint from which to consider cortical modularity. If this type of dense, unspecific connectivity pattern applies to other populations of cortical neurons, neighboring neurons would have overlapping but not identical connectivity patterns. In this scenario, there would be no modules in the cortical microcircuit, but instead each individual neuron defines its own circuit, based on its own distinct input and output innervation. Like in neural networks, each neuron could functionally reassemble its connectivity according to learning rules and previous activity patterns, and, in doing so, form part of different emergent functional units, such as neuronal assemblies (Hebb, 1949) or circuit attractors (Hopfield, 1982).

EXPERIMENTAL PROCEDURES

Slice Preparation and Electrophysiology

Three hundred fifty micrometer thick coronal slices from P11- to P41-day-old GIN transgenic mice (Oliva et al., 2000) frontal cortex were prepared using a Leica VT1000-S vibratome with a solution containing (in mM): 27 NaHCO₃, 1.5 NaH₂PO₄, 222 sucrose, 2.6 KCl, 2 MgSO₄, 2 CaCl₂. Slices were incubated at 32°C in ACSF (pH 7.4), containing (in mM): 126 NaCl, 3 KCl, 2 MgSO₄, 2 CaCl₂, 1 NaH₂PO₄, 26 NaHCO₃, and 10 glucose and saturated with 95% O₂ and 5% CO₂, for 30 min and then kept at room temperature for at least 30 min before transferring them to the recording chamber.

Whole-cell electrodes (4 to 7 M Ω) were used. Current-clamp recordings were performed with intracellular solution (pH 7.3), containing (in mM): 135 K-methylsulfate, 10 KCl, 10 HEPES, 5 NaCl, 2.5 Mg-ATP, 0.3 Na-GTP, and 0.1 Alexa Fluor 594. Voltage-clamp recordings were done with intracellular solution (pH 7.3), containing (in mM): 128 Cs-methanesulfonate, 10 HEPES,

2 MgCl₂, 2 MgSO₄, 4 Na₂-ATP, 0.4 Na-GTP, 10 Na₂-phosphocreatine and 0.1 Alexa Fluor 594. Neurons were either held at their resting membrane potential (sGFP cells), or at +40 mV and –40 mV (PCs). PC pairs current-clamp recordings were made with Cs-based internal (see Supplemental Experimental Procedures). Experiments were conducted at room temperature (22°C to 25°C) to prolong the life of the slices. We performed recordings using MultiClamp 700B (Molecular Devices) amplifiers and acquired the signals through a National Instruments PCI 6259 board using custom software developed with LABView (National Instruments).

Imaging and RuBi-Glutamate Uncaging

Images were acquired using a custom-made two-photon microscope based on the Olympus FV-200 system (side-mounted to a BX50WI microscope with a 40 \times , 0.8 NA, or 20 \times , 0.5 NA, water immersion objectives) and a Ti:sapphire laser (Chameleon Ultra II, Coherent, >3 W, 140 fs pulses, 80 MHz repetition rate). Fluorescence was detected with a photomultiplier tube (PMT: H7422-P40 Hamamatsu) connected to a signal amplifier (Signal Recovery AMETEK Advanced Measurement Technology). Images were acquired with Fluoview software (XY scan mode with 1 \times to 10 \times digital zoom), at 850 nm for Alexa 594 and 900 nm for GFP, using minimal power to prevent RuBi-Glutamate uncaging.

RuBi-Glutamate (TOCRIS) was added to the bath at 300 μ M concentration. This concentration chosen for two-photon experiments was the lowest concentration with which we were able to fire reliably using our stimulation protocol. A somatic uncaging point was selected using custom software (Nikolenko et al., 2007). RuBi-Glutamate was excited at 800 nm for uncaging. Laser power was modulated by a Pockels cell (Conoptics). For somatic stimulations, each neuron was stimulated with a circular array of 8 subtargets, each of which was illuminated for 8 ms, giving a total duration of ~70 ms. The subtargets themselves consisted of 5 very closely spaced beamlets created by multiplexing the laser beam with a diffractive optical element (DOE) (Nikolenko et al., 2007). Typical power levels on sample were 230 \pm 80 mW (40 \times , 0.8 NA objective) or 170 \pm 60 mW (20 \times , 0.5 NA objective). We usually evoked bursts of APs to ensure detecting connections. Successive neuronal targets were stimulated every second; this rapid neuron to neuron stimulation allowed us to quickly assess the connectivity of multiple neuronal pairs using the “switching test” (see Results). Occasionally, responses were “mixed,” composed of outward and inward currents at –40 mV. Since the purpose of our study was to detect all potential inhibitory connections, we tallied these responses as inhibitory for our analysis, because they did reveal the existence of an inhibitory connection. All maps with paired or triple recordings were acquired with a 20 \times objective (0.5 NA); the investigated fields represented around 600 \times 800 μ m, including therefore layers 2/3 and 1.

Biocytin Histochemistry and Reconstructions

Neurons were filled with biocytin (5 mg/ml; Sigma) by the patch pipette. Subsequently, slices were fixed overnight in 4% paraformaldehyde in 0.1 M phosphate buffer at 4°C. Biocytin-filled cells were visualized using the avidin-biotin-horseradish peroxidase reaction. Successfully filled and stained neurons were then reconstructed using NeuroLucida (MicroBrightField) (see details in Supplemental Experimental Procedures).

Data Analysis

Off-line analysis was conducted using Matlab or Igor Pro with the Neuromatic v2.0 package. All results are expressed as mean \pm SEM. Statistical significance was assessed using Student’s t test, Mann-Whitney, and Wilcoxon tests or one-way ANOVA at the significance level (p) indicated. Analysis of electrophysiological properties of interneuron and characteristics of synaptic transmission are detailed in the Supplemental Experimental Procedures.

SUPPLEMENTAL INFORMATION

Supplemental Information includes three figures and Supplemental Experimental Procedures and can be found with this article online at doi:10.1016/j.neuron.2011.02.025.

ACKNOWLEDGMENTS

We thank V. Nikolenko for inspiration and help, L. McGarry, Y. Shin, and J. Miller for anatomical reconstructions, M. Dar for help with mice, L. McGarry for cluster analysis and D. Rabinowitz and members of the laboratory for help and comments. Supported by the Kavli Institute for Brain Science, the National Eye Institute, and the Marie Curie IOF Program.

Accepted: December 13, 2010

Published: March 23, 2011

REFERENCES

- Ascoli, G.A., Alonso-Nanclares, L., Anderson, S.A., Barrionuevo, G., Benavides-Picciono, R., Burkhalter, A., Buzsáki, G., Cauli, B., Defelipe, J., Fairén, A., et al; Petilla Interneuron Nomenclature Group. (2008). Petilla terminology: Nomenclature of features of GABAergic interneurons of the cerebral cortex. *Nat. Rev. Neurosci.* 9, 557–568.
- Berger, T.K., Perin, R., Silberberg, G., and Markram, H. (2009). Frequency-dependent disinhibition in the pyramidal network: A ubiquitous pathway in the developing rat neocortex. *J. Physiol.* 587, 5411–5425.
- Braitenberg, V., and Schüz, A. (1991). *Anatomy of the Cortex* (Berlin: Springer).
- Burkhalter, A. (1989). Intrinsic connections of rat primary visual cortex: Laminar organization of axonal projections. *J. Comp. Neurol.* 279, 171–186.
- Callaway, E.M. (1998). Local circuits in primary visual cortex of the macaque monkey. *Annu. Rev. Neurosci.* 21, 47–74.
- Callaway, E.M., and Katz, L.C. (1993). Photostimulation using caged glutamate reveals functional circuitry in living brain slices. *Proc. Natl. Acad. Sci. USA* 90, 7661–7665.
- Crick, F.H.C., and Asanuma, C. (1986). Certain aspects of the anatomy and physiology of the cerebral cortex. In *Parallel Distributed Processing*, J.L. McClelland and D.E. Rumelhart, eds. (Cambridge, MA: MIT Press), pp. 333–371.
- DeFelipe, J. (1993). Neocortical neuronal diversity: chemical heterogeneity revealed by colocalization studies of classic neurotransmitters, neuropeptides, calcium-binding proteins, and cell surface molecules. *Cereb. Cortex* 3, 273–289.
- Deuchards, J., West, D.C., and Thomson, A. (1994). Relationships between morphology and physiology of pyramid-pyramid single axon connections in rat neocortex in vitro. *J. Neurophysiol.* 478, 423–435.
- Douglas, R.J., Martin, K.A.C., and Markram, H. (2004). Neocortex. In *The Synaptic Organization of the Brain*, G.M. Shepherd, ed. (Oxford: Oxford University Press), pp. 499–558.
- Fagioli, M., and Hensch, T.K. (2000). Inhibitory threshold for critical-period activation in primary visual cortex. *Nature* 404, 183–186.
- Fairen, A., De Felipe, J., and Regidor, J. (1984). Nonpyramidal neurons. In *Cerebral Cortex*, A. Peters and E.G. Jones, eds. (New York: Plenum), pp. 201–253.
- Farber, I.C., and Grinvald, A. (1983). Identification of presynaptic neurons by laser photostimulation. *Science* 222, 1025–1027.
- Feldmeyer, D., and Sakmann, B. (2000). Synaptic efficacy and reliability of excitatory connections between the principal neurones of the input (layer 4) and output layer (layer 5) of the neocortex. *J. Physiol.* 525, 31–39.
- Fino, E., Araya, R., Peterka, D.S., Salierno, M., Etchenique, R., and Yuste, R. (2009). RuBi-glutamate: two-photon and visible-light photoactivation of neurons and dendritic spines. *Front. Neural Circuits* 3, 2.
- Gibson, J.R., Beierlein, M., and Connors, B.W. (1999). Two networks of electrically coupled inhibitory neurons in neocortex. *Nature* 402, 75–79.
- Gilbert, C.D., and Wiesel, T.N. (1979). Morphology and intracortical projections of functionally characterised neurones in the cat visual cortex. *Nature* 280, 120–125.
- Goldberg, J.H., Lacefield, C.O., and Yuste, R. (2004). Global dendritic calcium spikes in mouse layer 5 low threshold spiking interneurons: implications for control of pyramidal cell bursting. *J. Physiol.* 558, 465–478.
- Gonchar, Y., and Burkhalter, A. (1997). Three distinct families of GABAergic neurons in rat visual cortex. *Cereb. Cortex* 7, 347–358.
- Gonchar, Y., Turney, S., Price, J.L., and Burkhalter, A. (2002). Axi-axonic synapses formed by somatostatin-expressing GABAergic neurons in rat and monkey visual cortex. *J. Comp. Neurol.* 443, 1–14.
- Grinvald, A., Frostig, R.D., Lieke, E., and Hildesheim, R. (1988). Optical imaging of neuronal activity. *Physiol. Rev.* 68, 1285–1366.
- Gupta, A., Wang, Y., and Markram, H. (2000). Organizing principles for a diversity of GABAergic interneurons and synapses in the neocortex. *Science* 287, 273–278.
- Halabisky, B., Shen, F., Huguenard, J.R., and Prince, D.A. (2006). Electrophysiological classification of somatostatin-positive interneurons in mouse sensorimotor cortex. *J. Neurophysiol.* 96, 834–845.
- Hebb, D.O. (1949). *The Organization of Behaviour* (Hoboken, NJ: Wiley).
- Hopfield, J.J. (1982). Neural networks and physical systems with emergent collective computational abilities. *Proc. Natl. Acad. Sci. USA* 79, 2554–2558.
- Hubel, D.H. (1988). *Eye, Brain and Vision* (New York: Scientific American Library).
- Hubel, D.H., and Wiesel, T.N. (1974). Uniformity of monkey striate cortex: A parallel relationship between field size, scatter, and magnification factor. *J. Comp. Neurol.* 158, 295–305.
- Hubel, D.H., and Wiesel, T.N. (1977). Ferrier lecture. Functional architecture of macaque monkey visual cortex. *Proc. R. Soc. Lond. B Biol. Sci.* 198, 1–59.
- Isseroff, A., Schwartz, M.L., Dekker, J.J., and Goldman-Rakic, P.S. (1984). Columnar organization of callosal and associational projections from rat frontal cortex. *Brain Res.* 293, 213–223.
- Kalisman, N., Silberberg, G., and Markram, H. (2005). The neocortical microcircuit as a tabula rasa. *Proc. Natl. Acad. Sci. USA* 102, 880–885.
- Kampa, B.M., Letzkus, J.J., and Stuart, G.J. (2006). Cortical feed-forward networks for binding different streams of sensory information. *Nat. Neurosci.* 9, 1472–1473.
- Kapfer, C., Glickfeld, L.L., Atallah, B.V., and Scanziani, M. (2007). Supralinear increase of recurrent inhibition during sparse activity in the somatosensory cortex. *Nat. Neurosci.* 10, 743–753.
- Katz, L.C., and Shatz, C.J. (1996). Synaptic activity and the construction of cortical circuits. *Science* 274, 1133–1138.
- Katzel, D., Zemelman, B.V., Buetfering, C., Wolfel, M., and Miesenböck, G. (2010). The columnar and laminar organization of inhibitory connections to neocortical excitatory cells. *Nat. Neurosci.* 14, 100–107.
- Kawaguchi, Y. (1995). Physiological subgroups of nonpyramidal cells with specific morphological characteristics in layer II/III of rat frontal cortex. *J. Neurosci.* 15, 2638–2655.
- Kawaguchi, Y., and Kubota, Y. (1997). GABAergic cell subtypes and their synaptic connections in rat frontal cortex. *Cereb. Cortex* 7, 476–486.
- Kerlin, A.M., Andermann, M.L., Berezovskii, V.K., and Reid, R.C. (2010). Broadly tuned response properties of diverse inhibitory neuron subtypes in mouse visual cortex. *Neuron* 67, 858–871.
- Kozloski, J., Hamzei-Sichani, F., and Yuste, R. (2001). Stereotyped position of local synaptic targets in neocortex. *Science* 293, 868–872.
- LeBon-Jego, M., and Yuste, R. (2007). Persistently active, pacemaker-like neurons in primary visual cortex. *Front. Neurosci.* 1, 123–129.
- Lorente de Nó, R. (1949). Cerebral cortex: architecture, intracortical connections, motor projections. In *Physiology of the Nervous System*, J.F. Fulton, ed. (New York: Oxford University Press), pp. 228–330.
- Markram, H., Lübke, J., Frotscher, M., Roth, A., and Sakmann, B. (1997). Physiology and anatomy of synaptic connections between thick tufted pyramidal neurones in the developing rat neocortex. *J. Physiol.* 500, 409–440.
- Matsuzaki, M., Honkura, N., Ellis-Davies, G.C., and Kasai, H. (2004). Structural basis of long-term potentiation in single dendritic spines. *Nature* 429, 761–766.

- McGarry, L.M., Packer, A.M., Fino, E., Nikolenko, V., Sippy, T., and Yuste, R. (2010). Quantitative classification of somatostatin-positive neocortical interneurons identifies three interneuron subtypes. *Front. Neural Circuits* 4, 12.
- Mountcastle, V.B. (1982). An organizing principle of cerebral function: The unit module and the distributed system. In *The Mindful Brain*, H.O. Schmitt, ed. (Cambridge, MA: MIT Press), pp. 1–50.
- Mountcastle, V.B. (1998). *Perceptual Neuroscience: The Cerebral Cortex* (Cambridge, MA: Harvard University Press).
- Murayama, M., Pérez-Garci, E., Nevian, T., Bock, T., Senn, W., and Larkum, M.E. (2009). Dendritic encoding of sensory stimuli controlled by deep cortical interneurons. *Nature* 457, 1137–1141.
- Nikolenko, V., Poskanzer, K.E., and Yuste, R. (2007). Two-photon photostimulation and imaging of neural circuits. *Nat. Methods* 4, 943–950.
- Oliva, A.A., Jr., Jiang, M., Lam, T., Smith, K.L., and Swann, J.W. (2000). Novel hippocampal interneuronal subtypes identified using transgenic mice that express green fluorescent protein in GABAergic interneurons. *J. Neurosci.* 20, 3354–3368.
- Otsuka, T., and Kawaguchi, Y. (2009). Cortical inhibitory cell types differentially form intralaminar and interlaminar subnetworks with excitatory neurons. *J. Neurosci.* 29, 10533–10540.
- Peinado, A., Yuste, R., and Katz, L.C. (1993). Extensive dye coupling between rat neocortical neurons during the period of circuit formation. *Neuron* 10, 103–114.
- Peters, A., and Jones, E.G. (1984). *Cerebral Cortex, Volume 1–13* (New York: Plenum).
- Peters, A., Paley, S.L., and Webster, H.F. (1976). *The Fine Structure of the Nervous System* (Philadelphia: Saunders).
- Rolls, E.T., and Treves, A. (1998). *Neural Networks and Brain Function*, First Edition (Oxford: Oxford University Press).
- Runyan, C.A., Schummers, J., Van Wart, A., Kuhlman, S.J., Wilson, N.R., Huang, Z.J., and Sur, M. (2010). Response features of parvalbumin-expressing interneurons suggest precise roles for subtypes of inhibition in visual cortex. *Neuron* 67, 847–857.
- Silberberg, G., and Markram, H. (2007). Disynaptic inhibition between neocortical pyramidal cells mediated by Martinotti cells. *Neuron* 53, 735–746.
- Somogyi, P., Tamás, G., Lujan, R., and Buhl, E.H. (1998). Salient features of synaptic organisation in the cerebral cortex. *Brain Res. Brain Res. Rev.* 26, 113–135.
- Stepanyants, A., Hof, P.R., and Chklovskii, D.B. (2002). Geometry and structural plasticity of synaptic connectivity. *Neuron* 34, 275–288.
- Thomson, A.M., and Lamy, C. (2007). Functional maps of neocortical local circuitry. *Front. Neurosci.* 1, 19–42.
- Thomson, A.M., and Morris, O.T. (2002). Selectivity in the inter-laminar connections made by neocortical neurones. *J. Neurocytol.* 31, 239–246.
- Thomson, A.M., Girdlestone, D., and West, D.C. (1988). Voltage-dependent currents prolong single-axon postsynaptic potentials in layer III pyramidal neurons in rat neocortical slices. *J. Neurophysiol.* 60, 1896–1907.
- Thomson, A.M., West, D.C., Wang, Y., and Bannister, A.P. (2002). Synaptic connections and small circuits involving excitatory and inhibitory neurons in layers 2–5 of adult rat and cat neocortex: Triple intracellular recordings and biocytin labelling in vitro. *Cereb. Cortex* 12, 936–953.
- Wang, Y., Toledo-Rodriguez, M., Gupta, A., Wu, C., Silberberg, G., Luo, J., and Markram, H. (2004). Anatomical, physiological and molecular properties of Martinotti cells in the somatosensory cortex of the juvenile rat. *J. Physiol.* 561, 65–90.
- Xu, X., and Callaway, E.M. (2009). Laminar specificity of functional input to distinct types of inhibitory cortical neurons. *J. Neurosci.* 29, 70–85.
- Xu, Q., Cobos, I., De La Cruz, E., Rubenstein, J.L., and Anderson, S.A. (2004). Origins of cortical interneuron subtypes. *J. Neurosci.* 24, 2612–2622.
- Yoshimura, Y., and Callaway, E.M. (2005). Fine-scale specificity of cortical networks depends on inhibitory cell type and connectivity. *Nat. Neurosci.* 8, 1552–1559.
- Yoshimura, Y., Dantzker, J.L., and Callaway, E.M. (2005). Excitatory cortical neurons form fine-scale functional networks. *Nature* 433, 868–873.
- Yuste, R. (2005). Origin and classification of neocortical interneurons. *Neuron* 48, 524–527.